Electric-field gradients at the ^{181}Ta impurity site in Yb, Y, and Dy sesquioxides

A. F. Pasquevich,* A. G. Bibiloni,† C. P. Massolo,† M. Rentería,† and J. A. Vercesi
Departamento de Física, Facultad de Ciencias Exactas, Universidad Nacional de La Plata, c.c. No. 67, 1900 La Plata, Argentina

K. Freitag
Institut für Strahlen- und Kernphysik, der Universität Bonn, Nussallee 14-16, 5300 Bonn, Germany
(Received 21 September 1993; revised manuscript received 14 February 1994)

The perturbed-angular-correlation (PAC) technique has been applied to the study of the internal electric-field gradients (EFG) in Yb, Y, and Dy sesquioxides. The ^{181}Ta PAC probes were introduced in the oxide lattices by means of ^{181}Hf implantation, which decays to the Ta impurity by β emission. The tracer ^{181}Ta was used and the results were compared to those obtained in bixbyite-structure compounds using ^{111}Cd as a probe. The measured EFG are essentially independent from the probe, reflecting the structure characteristics of both crystalline sites in these compounds. In the case of $^{181}Hf^{4+}$ and $^{181}Ta^{5+}$, charge compensation (the cations are 3+) seems to be accomplished through a uniform distribution of the probe's extra electrons in the neighboring oxygen anions. Comparisons of the results to point-charge model predictions are also discussed.

I. INTRODUCTION

The perturbed-angular-correlation technique (PAC) has been extensively used for the hyperfine characterization of the electric-field gradients (EFG) at impurity lattice sites in binary oxides. The PAC technique is based on the observation of the influence of extranuclear fields on the correlation between emission directions of two successive radiations emitted during a nuclear decay cascade. The method requires the introduction of an appropriate radiative probe in substitutional cation sites of the lattice. Through the measurement of the quadrupole frequency ω_Q and the asymmetry parameter η, the *EFG* at the site of the nucleus of the probe can be determined if the nuclear quadrupole moment of the intermediate level of the cascade is known. Up to now the literature shows frequently the use of ^{111}In/^{111}Cd as probes and less frequently that of ^{181}Hf/^{181}Ta. From the cumulated data several attempts to correlate experimental results and theoretical calculations were done.[1,2] Recently a well-defined correlation between local and lattice contributions of the *EFG* was presented for ^{111}Cd in binary oxides.[3] The local component of the *EFG* in binary oxides, originated in extraionic contributions, is extracted from all quadrupole coupling constants measured in PAC experiments with ^{111}Cd probes. The resulting systematic reveals a linear dependence of the local component on the ionic one, over a wide range of ionic *EFG* values, both contributing with opposite signs.

Among the binary oxides, the sesquioxides that crystallize in the bixbyite structure were the subject of several investigations using ^{111}Cd.[4] This group is of particular interest since it includes rare-earth cations as well as a wide range of lattice constants, from 10 to 11 Å. Also the presence of two similar but inequivalent lattice sites for cations with quite different asymmetry parameters make them a useful tool for the understanding of the behavior of the *EFG* at impurity sites.

To our knowledge, only two sesquioxides, In_2O_3 (Ref. 5) and Y_2O_3 (Ref. 6) have been studied using ^{181}Ta as a probe. It seems then of importance to extend these investigations, if comparison with existent results for ^{111}Cd are to be done.

An interesting difference between experiments using ^{111}In and ^{181}Hf in these oxides appears from the different valence of both impurities. Indium is isovalent with the cations of the host lattice, while hafnium is a donor impurity. The question of charge compensation arises in the last case. The compensation can occur by the appearance of a lattice defect or by a change in the state of charge of the ions in the neighborhood of the impurity. The PAC technique is quite appropriate for distinguishing between both cases. The problematic of the compensation has been recently investigated both experimentally and theoretically in the system Y_2O_3:Zr,[7] which is quite comparable to the ones reported in this paper.

With these aims we performed PAC experiments in three sesquioxides, namely Yb_2O_3, Y_2O_3, and Dy_2O_3 using ^{181}Ta as a probe. We characterized these oxides through their hyperfine parameters at room temperature and finally compared them to those obtained using ^{111}Cd as the probe. The results verified the structure characteristics of both crystalline sites. A comparison with the results obtained for Cd reveal that the existent electric-field gradients are essentially independent of the impurity in these bixbyite oxides.

We have also tried to compare our results to those existing in the literature obtained both with PAC and Mössbauer spectroscopy using a variety of rare-earth probes in these sesquioxides. In spite of the difficulties that arise from the fact that in many cases only information about one site is available, the possibility of evalu-

ating the $4f$ electron contribution to the EFG appears, through the comparison to the results coming from closed inner shells probes. All these features are discussed in Sec. V.

II. THE BIXBYITE STRUCTURE

This group takes its name from the mineral $(Fe,Mn)_2O_3$, called bixbyite. The cations forms a nearly cubic face center lattice in which six out of the eight tetrahedral sites are occupied by oxygens. The elementary cell of the oxide lattice consists of eight such cubes, containing 32 cations and 48 O^{2-} ions. The structure is characterized by two inequivalent sites for the cations, called "C" and "D," both O_6-coordinated as has been said. Their abundance in the lattice is 3:1. Site D is axially symmetric and can be described as surrounded by six oxygens at the corners of a distorted cube, leaving two corners on the same diagonal free. In site C the cube is more distorted and the six oxygens leave free two corners on a face diagonal. Point-charge model (PCM) calculations led to asymmetry parameters η_D of 0.0 and η_C from 0.7 to 1.0.

In Fig. 1, we represent the distribution of the first-neighbor oxygens around the cations in each site. The real situation has been approximated by a cube and can be thought of as a base for the analysis of each bixbyite. This approximation keeps the main symmetry properties of the sites. PCM calculations performed assuming equal charge q for each nearest-neighbor (NN) oxygen ion give 0.0 and 1.0 for the asymmetry parameters of sites D and C, respectively. In this approximation, the predicted ratio between the electric-field gradient V_{zz} for site C and D is independent of the lattice parameter "a" and equal to 0.5.

III. EXPERIMENT

Pressed pills of high purity oxides were ion implanted at the Institut für Strahlen- und Kernphysik. The ^{181}Hf $-\beta^- \rightarrow {}^{181}$Ta activity was implanted at 150 KeV. The total calculated doses were approximately 10^{13} ions/cm^2.

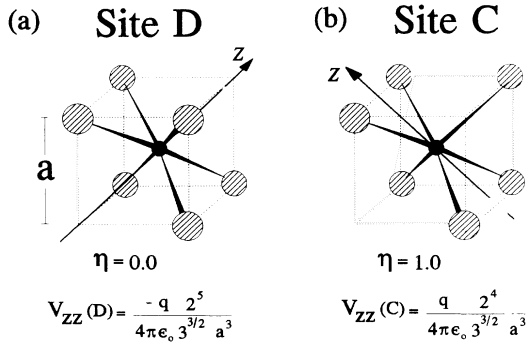

FIG. 1. Oversimplified scheme of the oxygen distribution around each cationic site in the bixbyite structure: (a) site D, (b) site C. The arrow denotes the EFG principal component direction in each situation. V_{zz} and η values, calculated assuming equal charge q the oxygen ions, are also quoted in each case. In the real structures the oxygens are slightly displaced from the corners of the cube.

The hyperfine interactions were observed by means of the PAC technique, which has been extensively described in the literature,[8] using the well-known 133–482 keV γ-γ cascade of ^{181}Ta. The angular correlation of these gamma rays is perturbed if there are external fields acting on the intermediate nuclear level. These fields appear in the perturbation factor $G_2(t)$, where t is the time spent by the nucleus in the intermediate level of the cascade. In the present case, the measurements were performed on a conventional four detector apparatus with BaF_2 scintillators with the detectors arranged in a plane at 90° angular intervals. The time resolution of the experimental set up was 0.9 ns (full width at half maximum of the prompt peak). Eight coincidence spectra between both γ rays, $C_{ij}(t)$, were simultaneously recorded. $C_{ij}(t)$ is the number of events in which the first γ ray enters detector i and after a time t the second enters detector j. After correction for accidental coincidences the eight spectra were combined to form the asymmetry ratio $R(t)$

$$R(t) = 2\frac{[(C_{13}C_{24})^{1/2} - (C_{14}C_{23})^{1/2}]}{[(C_{13}C_{24})^{1/2} + 2(C_{14}C_{23})^{1/2}]} = A_{22}^{\exp} G_2(t) \ . \tag{1}$$

Theoretical functions of the form $A_2^{\exp}G_2(t)$, $A_2^{\exp}$ being the effective anisotropy of the cascade, folded with the time resolution curve, were fitted to the experimental $R(t)$ asymmetry ratio.

For polycrystalline samples and a nuclear spin $I = 5/2$ of the intermediate level of the cascade, the perturbation factor $G_2(t)$ for static electrical quadrupole interactions has the form

$$G_2(t) = \sum_i f_i \left(S_{20,i} + \sum_{n=1}^{3} [S_{2n,i} \cos(\omega_{ni} t) e^{-\delta_i \omega_{ni} t}] \right) \ , \tag{2}$$

where f_i are the relative fractions of nuclei that experience a given perturbation. The ω_n frequencies are related to the quadrupole frequency $\omega_Q = eQV_{zz}/40\hbar$ by $\omega_n = g_n(\eta)\omega_Q$. The g_n and S_n coefficients are known functions[9] of the axial-asymmetry parameter $\eta = (V_{xx} - V_{yy})/V_{zz}$, where V_{ii} are the principal components of the EFG tensor and $|V_{xx}| \leq |V_{yy}| \leq |V_{zz}|$. The exponential functions account for a Lorentzian frequency distribution of relative width δ around ω_n.

IV. RESULTS

Figures 2 and 3 show the PAC spectra taken on each sample at room temperature as implanted and after 1 h thermal treatment at 1173 K in air. Their corresponding Fourier transforms are shown as well. The solid lines in the $R(t)$ spectra result from a least-squares fit of Eq. (2) to the data. The values of the hyperfine parameters are listed in Table I. Solid lines in the Fourier spectra come from the Fourier transform of the $R(t)$ fits. As can be seen, possible radiation damage is removed after the treatment and the probes rest, finally, at regular lattice

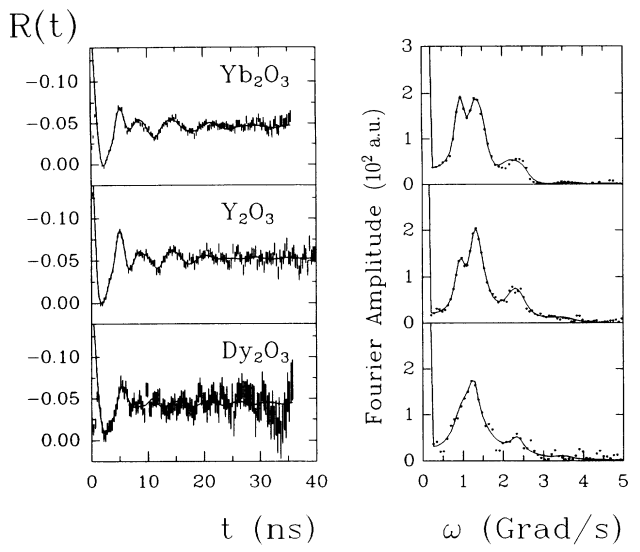

FIG. 2. PAC spectra of ^{181}Hf/^{181}Ta in Yb_2O_3, Y_2O_3, and Dy_2O_3 measured at RT as implanted. Solid lines indicate the least-squares fits of Eq. (2) to the data. Fourier transforms of the PAC spectra are shown to the right.

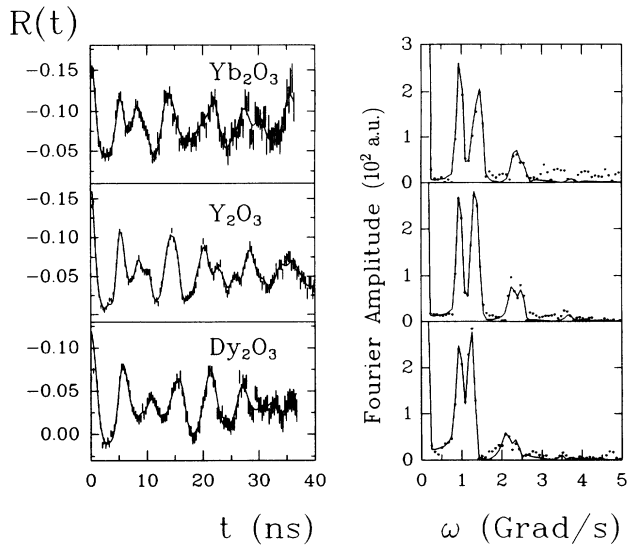

FIG. 3. PAC spectra of ^{181}Hf/^{181}Ta in Yb_2O_3, Y_2O_3, and Dy_2O_3 measured after an annealing treatment at 1173 K in air for 1 h. Solid lines indicate the least-squares fits of Eq. (2) to the data. Fourier transforms of the PAC spectra are shown to the right.

sites. Two seemingly monochromatic hyperfine interactions are present in the spectra, connected with the two inequivalent cation lattice sites. From the value of the fitted parameters displayed in the table we can see that the thermal annealing had two main consequences: it diminishes drastically the frequency distributions δ in both sites and at the same time reduces the value of the asymmetry parameter η_1. After these major changes the interactions can be undoubtedly associated to the crystalline sites called D and C in Sec. II. In effect, while the relation in the population factors f_i are approximately 1/3, the asymmetry parameters correspond to the expected symmetries and agree with the calculated ones (see Sec. II). Finally, the frequency associated to the axially symmetric interaction is higher than the asymmetric one as found previously with the ^{111}Cd probe and as predicted by PCM calculations.

V. DISCUSSION

The obtained results, displayed in Table I, show that the ^{181}Ta ions occupy two different lattice sites that should be associated to the cation sites D and C in the bixbyite structure.

Accordingly, with point-charge model predictions the highest frequency corresponds to the more symmetric and less populated site.

A comparison of the present results and those obtained with the probe ^{111}Cd in these and other isostructural compounds is shown in Fig. 4. To get rid of factors inherent to the probes, such as the Sternheimer factor and the nuclear quadrupole moment, the relation ω_{Q2}/ω_{Q1} is plotted as function of the host lattice parameter a. The straight line in this figure accounts for a regular dependence of the experimental results obtained with the

TABLE I. Results of least-squares fits of Eq. (2) to the data displayed in Figs. 2 and 3.

	Site D				Site C			
Oxide	f_1 (%)	ω_{Q1} (Mrad/s)	η_1	δ_1 (%)	f_2 (%)	ω_{Q2} (Mrad/s)	η_2	δ_2 (%)
Yb_2O_3								
As implanted	56_2	209_2	0.36_1	11.8_7	44_2	109.0_9	0.61_1	11.0_7
After 1173 K	35_5	209_2	0.01_4	3_1	65_5	122.6_5	0.47_1	1.6_4
Y_2O_3								
As implanted	68_5	195_1	0.27_2	12_1	32_5	125_2	0.39_3	14_2
After 1173 K	36_2	204.9_6	0.04_4	1.5_3	64_2	116.8_3	0.536_4	1.9_2
Dy_2O_3								
As implanted	24_{23}	193_7	0.19_8	6_5	76_{23}	121_{20}	0.5_2	27_9
After 1173 K	31_5	195.1_9	0.0_2	1.7_8	69_5	106.9_5	0.649_7	3.1_4

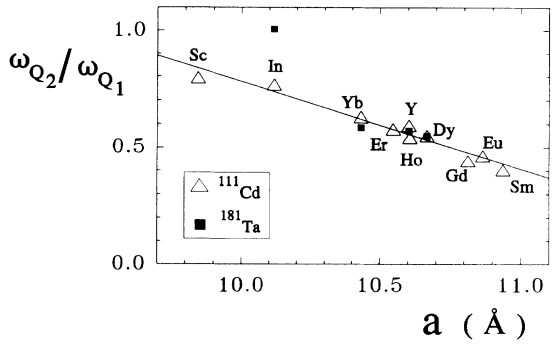

FIG. 4. Relation of sites C and D quadrupole frequencies present in bixbyites for ^{111}Cd and ^{181}Ta displayed as a function of the lattice parameter "a." Symbols denote data coming from measurements with open triangles from ^{111}Cd and black squares from ^{181}Ta. Solid line: linear fit to the ^{111}Cd data.

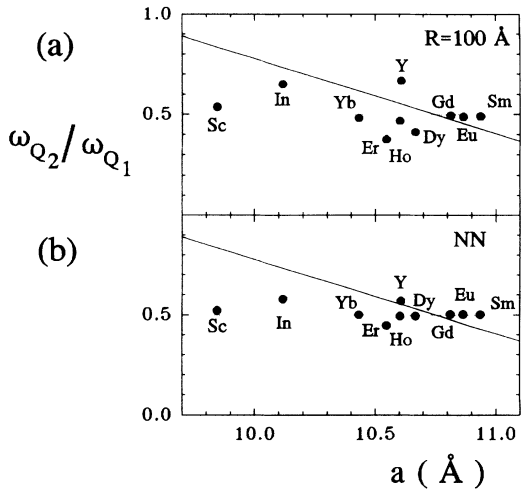

FIG. 5. Relation of sites C and D quadrupole frequencies calculated with the point-charge model for the bixbyites presented in Fig. 4 as a function of the lattice parameter "a": (a) contribution from ions within a sphere of radius $R = 100$ Å around the probe and (b) next-nearest-neighbor oxygen contribution. Dotted line: result for this relation in the idealized NN neighbors oxygen distribution around sites C and D, as shown in Fig. 1. Solid line: linear fit to the ^{111}Cd experimental data plotted in Fig. 4.

^{111}Cd probe. It can be seen that the present results for Ta agree as well. The results reported in Ref. 6 are not shown in Fig. 4 due to their rather high frequency distribution. The relation for the interactions in In_2O_3:Ta (Ref. 5) however, departs clearly from the other results. This is not surprising taking into account the distortion that Hf introduces in both sites of the indium sesquioxide lattice, as was previously reported.[5]

The fact that the relation of the interactions for both probes lies on the same line shows that they act as adequate observers of the charge distribution around regular lattice sites. Slight distortion of the sites cannot be excluded but since the asymmetry parameters remain essentially as expected, this distortion, if any, should imply just a contraction or expansion of the atomic distances, without a symmetry modification. In fact, such an atomic displacement has already been observed in Zr doped Y_2O_3.[7] On the other hand, we could conclude that the charge compensation involves neither any near-neighbor lattice defect nor any electronic charge localization at a neighbor ion. The additional charge looks uniformly distributed among the neighbor anions.

Point-charge model calculations were also performed at both cationic inequivalent sites in all the sesquioxides shown in Fig. 4, in order to obtain the quadrupole frequencies ω_Q^{PCM} and the asymmetry parameters η^{PCM} in this simple picture. The calculus was performed taking into account the point-charge ion contribution within a sphere of radius $R = 100$ Å, in which the direct sum contribution to the V_{ij} components of the EFG tensor has largely converged (less than 0.1 % for the difference between the contribution of two succesive shells of ions). The lattice parameters and the atomic coordinates used for each oxide have been taken from the latest x-ray and neutron diffraction determinations quoted in the literature[10]. The same calculus was done for only the next-nearest-neighbor oxygen ion contribution. The PCM predictions for the analyzed quotients (see Fig. 5), show that the PCM alone is not adequate for describing the situation at the smaller lattice parameters. The point-charge description fails with decreasing lattice parameters probably due to the overlap between the charge distribution in the oxygen ions and the central atom. On the other hand, the dispersion of the calculated values could indicate that the data for the atomic positions quoted in the literature and used in the calculus may be erroneous as pointed out by Bartos *et al.*[11]

In addition, the coincidence of the ratios we are discussing (shown for Yb, Y, and Dy sesquioxides in Fig. 4) implies a relation for the frequencies measured for each site and each oxide with both PAC probes. In effect, in Fig. 6 we plotted the frequencies measured with ^{181}Ta as function of those measured with ^{111}Cd. As can be

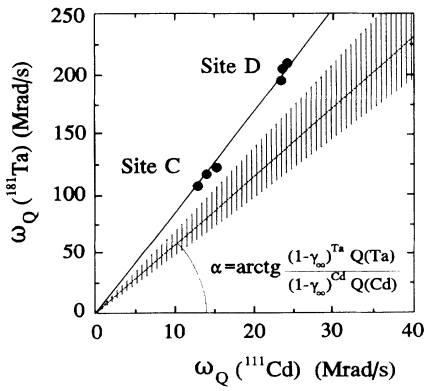

FIG. 6. Quadrupole frequencies ω_Q(Ta) measured with ^{181}Ta in sites D and C for Yb_2O_3, Y_2O_3, and Dy_2O_3, as function of those measured with ^{111}Cd. Solid line: linear fit to the data. Dash line: point-charge model prediction; its slope is quoted. Dotted lines: denotes the uncertainty in the PCM prediction due to experimental errors in the Q values.

seen, there is a linear relation between the interactions measured with both probes. The solid line in this figure is the result of a linear fit to the data and corresponds to

$$\frac{\omega_Q(\mathrm{Ta})}{\omega_Q(\mathrm{Cd})} = 8.48 \, . \tag{3}$$

It should be interesting to compare this experimental slope with the value expected in the PCM. In this model, the expected quadrupole frequency should be given by

$$\omega_Q = (1-\gamma_\infty)\frac{eQV_{zz}^{\mathrm{lattice}}}{40\hbar} \, . \tag{4}$$

The dashed line in Fig. 6 corresponds to the ratio

$$\frac{\omega_Q(\mathrm{Ta})_i}{\omega_Q(\mathrm{Cd})_i} = \frac{(1-\gamma_\infty)^{\mathrm{Ta}}Q(\mathrm{Ta})}{(1-\gamma_\infty)^{\mathrm{Cd}}Q(\mathrm{Cd})} = 5.86 \, , \tag{5}$$

where γ_∞^i and $Q(i)$ are the Sternheimer factors[12] and the nuclear quadrupole moments of the intermediate level of the cascade, respectively. The uncertainty in this ratio, due to the experimental error in the probes Q values, is represented by the dashed region between the dotted lines. The discrepancy between the experiment and the PCM prediction can be associated with the incomplete description of the EFG involved in Eq. (4). In effect, in the expression of Eq. (4), the local contribution to the EFG has not been taken into account (see Ref. 3).

As we anticipate in the Introduction, it could be interesting to consider in the present discussion the information available on EFG observed using other probes in the oxides analyzed here. We have looked for such results in the literature and found that although there are many papers on Mössbauer spectroscopy and PAC experiments using rare-earth probes in the bixbyite oxides, the results cannot be compared straightforward with the ones discussed above.

There is information of PAC experiments in sesquioxides using probes such as ^{161}Dy (Ref. 13) and ^{172}Yb (Ref. 14) but the quality of the results, due to the characteristics of the probes, did not allow the authors to obtain the quadrupole interaction parameters for the two sites. Something similar occurs in many Mössbauer experiments using rare earth isotopes where the accuracy and the resolution seems not to be good enough for an accurate analysis of the hyperfine fields.[15] There, the spectra were fitted by assuming only one pure electric interaction with $\eta \neq 0$ and the other site was neglected.

On the other hand, in the cases where the two sites were identified and the comparison could be attempted, the existence of the partly filled $4f$ shell and the low temperature used for the measurement result in a very important EFG contribution V_{zz}^{4f} which does not exist in the case of the probes ^{111}Cd and ^{181}Ta having inner closed electronic shells.

In order to show the importance of the $4f$ contribution as compared with the lattice contribution we will compare the EFG measured in Yb_2O_3 using the probes Cd, Ta, and Yb. In Table II the values V_{zz}^{exp} measured at the nucleus position and the lattice contribution to the EFG calculated by the PCM, enhanced by the antishielding Sternheimer factor γ_∞, are given. The calculated values approach much better the experimental results in the case of the Cd and Ta probes. In the case of the Yb, the difference between the measured value and $V_{zz}^{\mathrm{latt}}(1-\gamma_\infty)$ can be attributed to the contribution of the partly filled $4f$ shell. The difference for site C is in good agreement with the $4f$-shell contribution calculated by Plingen *et al.*[15]

Finally, from the analyzed results it can be seen that the $4f$ contribution is very important at both sites. It determines the value and the symmetry of the EFG. The change in the symmetry is apparent when the values for η^{exp}, quoted in Table II, are confronted with those predicted by the crystalline symmetries. It would be interesting to have a reliable evaluation of the $4f$ contribution in each site in order to see if the Cd and Ta characteristics as EFG observers could be extended to the rare-earth probes. Such investigations are in progress.

VI. CONCLUSIONS

The obtained results show that in spite of the different electronic configuration for the two probes, ^{111}In and ^{181}Hf, considered as free atoms and other differences with the atoms of the hosts, the measured electric-field gradi-

TABLE II. Comparison between experimental and calculated EFG parameters for ^{111}Cd, ^{181}Ta, and the rare-earth Yb for both sites of Yb_2O_3. Electric-field gradients are in units of 10^{17} V/cm^2.

		Site D			Site C		
Probe	γ_∞ [a]	V_{zz}^{exp}	$(1-\gamma_\infty)V_{zz}^{\mathrm{latt}}$	η^{exp}	V_{zz}^{exp}	$(1-\gamma_\infty)V_{zz}^{\mathrm{latt}}$	η^{exp}
$^{111}Cd^{2+}$	−29.27	7.67_9 [b]	+7.66	0.00	4.83_5 [b]	−3.69	0.75_2
$^{181}Ta^{3+}$	−61.42	23.3_2 [b]	+15.79	0.01_4	13.67_6 [b]	−7.61	0.47_1
Yb^{3+} [c]	−80.53	-13_1	+20.63	0.6_1	-32_1	−9.95	0.1_1

[a]The Sternheimer antishielding factors are taken from Ref. 12. In the case of $Ta^{3+}(Yb^{3+})$, the value came from interpolation of $Hf^{4+}(Yb^{2+})$ and $W^{6+}(Hf^{4+})$ values.

[b]All these values present sign indetermination, because of the PAC technique.

[c]The experimental values quoted for the Yb^{3+} probe are a mean of the results obtained with the isotopes ^{170,171,172,174}Yb in Ref. 15.

ents at the crystalline sites in Yb_2O_3, Y_2O_3, and Dy_2O_3 are essentially independent of the impurity, reflecting their crystalline structure. These results allowed us to obtain the value of 8.48 for the ratio of the quadrupole interactions strengths between ^{181}Ta and ^{111}Cd.

Additionally, the way in which the charge compensation occurs has been discussed and a uniform distribution of the probe's extra electrons in the neighboring anions was observed.

ACKNOWLEDGMENTS

This work was partially supported by Consejo Nacional de Investigaciones Científicas y Técnicas (CONICET) and Comisión de Investigaciones Científicas de la Provincia de Buenos Aires (CICPBA), Argentina, Volkswagen Werkstiftung, Germany, and Third World Academy of Science (TWAS), Italy.

*Also at CIC Provincia de Buenos Aires, Argentina.
†Also at CONICET, Argentina.

[1] W. Bolse, A. Bartos, J. Kesten, M. Uhrmacher, and K. P. Lieb, *XXIII Zakopane School on Physics*, edited by K. Krolas and K. Tomala (Institute of Nuclear Physics, Cracow, 1988).

[2] J. Kesten, W. Bolse, K. P. Lieb, and M. Uhrmacher, Hyperfine Interact. **60**, 683 (1990).

[3] M. Rentería, C. P. Massolo, and A. G. Bibiloni, Mod. Phys. Lett. B **6**, 1819 (1992).

[4] EFG measurements with ^{111}Cd as the probe in bixbyite-structure sesquioxides. In_2O_3: J. Desimoni, A. G. Bibiloni, L. A. Mendoza-Zélis, A. F. Pasquevich, F. H. Sánchez, and A. R. López-García, Phys. Rev. B **28**, 5739 (1983); Y_2O_3: M. Uhrmacher, A. Bartos, and K. Winzer, J. Less-Common Metals **150**, 185 (1989); Yb_2O_3, Dy_2O_3, and Sc_2O_3: A. Bartos, K. P. Lieb, A. F. Pasquevich, M. Uhrmacher, and ISOLDE Collaboration, Phys. Lett. A **157**, 513 (1991); Ho_2O_3, Gd_2O_3, and Sm_2O_3: J. Shitu, D. Wiarda, T. Wenzel, M. Uhrmacher, K. P. Lieb, S. Bedi, and A. Bartos, Phys. Rev. B **46**, 7987 (1992); Er_2O_3 and Eu_2O_3: A. F. Pasquevich, A. M. Rodríguez, H. Saitovich, and P. R. de Jesus-Silva (unpublished).

[5] J. A. Vercesi, A. G. Bibiloni, C. P. Massolo, M. S. Moreno, A. F. Pasquevich, and K. Freitag, Phys. Rev. B **47**, 490 (1993).

[6] A. A. Sorokin, E. N. Shirani, L. G. Shpinkova, Z. Z. Akselrod, B. A. Komissarova, G. K. Ryasny, S. I. Semyonov, G. A. Denisenko, I. P. Zibrov, and A. R. Buev, Hyperfine Interact. **73**, 3370 (1992).

[7] N. Thromat, C. Noguera, M. Gautier, F. Yollet, and J. P. Durand, Phys. Rev. B **44**, 7904 (1991).

[8] H. Frauenfelder and R. M. Steffen, in *α, β and γ-Ray Spectroscopy*, edited by K. Siegbahn (North-Holland, Amsterdam, 1968), Vol. 2, p. 917.

[9] L. A. Mendoza-Zélis, A. G. Bibiloni, M. C. Caracoche, A. R. López-García, J. A. Martínez, R. C. Mercader, and A. F. Pasquevich, Hyperfine Interact. **3**, 315 (1977).

[10] Crystal structure data used in the PCM predictions. Two references are quoted if lattice parameters and atomic positions comes from different articles (lattice parameters articles are quoted first). In_2O_3: M. Marezio, Acta Crystallogr. **20**, 723 (1966); Y_2O_3: H. G. Scott, Acta Crystallogr. Sec. A **37**, 456 (1981); M. Bonnet, A. Delapalme, and H. Fuess, *ibid.* **31**, 264 (1975); Sm_2O_3, Gd_2O_3, and Er_2O_3: R. W. G. Wyckoff, *Crystal Structures* (Wiley Interscience, New York, 1964), Vol. 2; Ho_2O_3: R. W. G. Wyckoff *ibid.*; A. Fert, Bull. Soc. Franç. Minér. Crist. **85**, 267 (1962); Eu_2O_3: R. W. G. Wyckoff, *ibid.*, and G. Gashurov and O. J. Sovers, Acta Crystallogr. Sec. B **26**, 938 (1970); Sc_2O_3: R. W. G. Wyckoff, *ibid.*; R. Norrestam, Ark. Kemi. **29**, 343 (1968); Dy_2O_3: R. W. G. Wyckoff, *ibid.*; W. Hase, Phys. Status Solidi **3**, K446 (1963); Dy_2O_3: A. Saiko, N. Ishizawa, N. Mizutani, and M. Kato, Yogyo Kyokai Shi **93**, 649 (1985). These data can be found in G. Will, N. Masciocchi, M. Hart, and W. Parrish, Acta Crystallogr. Sec. A **43**, 677 (1987).

[11] A. Bartos, K. P. Lieb, M. Uhrmacher, and D. Wiarda, Acta Crystallogr. Sec. B **49**, 165 (1993).

[12] F. D. Feiock and W. R. Johnson, Phys. Rev. **187**, B39 (1969).

[13] G. A. Petitt and F. E. Obenshain, Phys. Rev. B **16**, 967 (1977).

[14] R. L. Rasera and A. Li-Scholz, Phys. Rev. B **1**, 1995 (1970).

[15] K.-G. Plingen, B. Wolbeck, and F.-J. Schröder, Nucl. Phys. A **165**, 97 (1971).